View metadata, citation and similar papers at core.ac.uk

brought to you by CORE

provided by Electronic Sumy State University Institutional Repository

JOURNAL OF NANO- AND ELECTRONIC PHYSICS
Vol. 4 No 1, 01016(6pp) (2012)

ЖУРНАЛ НАНО- ТА ЕЛЕКТРОННОЇ ФІЗИКИ
Том 4 № 1, 01016(6cc) (2012)

Analysis of the Band-Structure in (Ga, Mn)As Epitaxial Layers by Optical Methods

O. Yastrubchak*

Institute of Physics, Maria Curie-Skłodowska University,
Place Marii Curie-Skłodowskiej 1, 20-031 Lublin, Poland

(Received 31 October 2011; revised manuscript received 28 February 2012; published online 14 March 2012)

The ternary III-V semiconductor (Ga, Mn)As has recently drawn a lot of attention as the model diluted ferromagnetic semiconductor, combining semiconducting properties with magnetism. (Ga, Mn)As layers are usually gown by the low-temperature molecular-beam epitaxy (LT-MBE) technique. Below a magnetic transition temperature, T_C, substitutional Mn^{2+} ions are ferromagnetically ordered owing to interaction with spin-polarized holes. However, the character of electronic states near the Fermi energy and the electronic structure in ferromagnetic (Ga, Mn)As are still a matter of controversy. The photoreflectance (PR) spectroscopy was applied to study the band-structure evolution in (Ga, Mn)As layers with increasing Mn content. We have investigated thick (800-700 nm and 230-300 nm) (Ga, Mn)As layers with Mn content in the wide range from 0.001 % to 6 % and, as a reference, undoped GaAs layer, grown by LT-MBE on semi-insulating (001) GaAs substrates. Our findings were interpreted in terms of the model, which assumes that the mobile holes residing in the valence band of ferromagnetic (Ga, Mn)As and the Fermi level position determined by the concentration of valence-band holes.

Keywords: Spintronics, Diluted ferromagnetic semiconductor, Photoreflectance (PR) spectroscopy, Fermi level, (Ga, Mn)As.

PACS numbers: 71.20.Mq, 83.85.Ei

1. INTRODUCTION

There has been a considerable increase in the past decade in the research activity developing basic materials for spin electronics. Diluted ferromagnetic semiconductors, combining semiconductor properties with magnetism, are especially promising as the materials for spintronics. In this respect, (Ga, Mn)As has become a model ferromagnetic semiconductor prospective for integrating semiconductor-based information processing and magnetic-based data storage on the same chip because of its compatibility with the established GaAs-based semiconductor technology. Homogeneous films of $Ga_{1-x}Mn_xAs$ containing up to above 10 % of Mn atoms can be grown by low-temperature (200-250 °C) molecular-beam epitaxy (LT-MBE) [1]. When intentionally undoped the films are *p*-type, where Mn atoms, substituting Ga atoms in the GaAs crystal lattice, supply both mobile holes and magnetic moments.

On the other hand, undoped LT-MBE-grown GaAs (LT-GaAs) films are *n*-type, because during the growth an important amount of about 1 % excess arsenic is incorporated into the GaAs matrix in a form of arsenic antisites, As_{Ga}, arsenic interstitials, As_I, and gallium vacancies, V_{Ga} [2, 3]. These defects, mainly As_{Ga} with a typical concentration of 1×10^{20} cm^{-3}, result in electronic properties of LT-GaAs. The As_{Ga} defect acts as a double donor in GaAs giving rise to two deep energy levels in the band gap: the single donor level (0/+) at $E_C - 0.75$ eV and the double donor level (+/++) at $E_V + 0.52$ eV[4], where E_C and E_V are the conduction and valence band edges, respectively. In LT-GaAs the As_{Ga} levels broaden to form a deep donor band responsible for hopping conduction [3] and the Fermi level pinning at about 0.47 eV below the conduction band edge [5, 6]. Tunneling spectroscopy measurements revealed a band of donor states near $E_V = 0.5$ eV arising from the As_{Ga} defects, i.e. close to their double donor level, and the Fermi level, E_F, located above this band [7]. This situation, resulting from partial ionization of the As_{Ga}-related defect band by residual carbon acceptors and/or native V_{Ga} acceptors, is schematically shown in Fig. 1a [8].

Magnetic properties of (Ga, Mn)As films arise from the Mn spin system ($S_{Mn} = 5/2$ for Mn^{2+} charge state), which undergoes the ferromagnetic phase transition below the Curie temperature, T_C. Mn atoms substituting the Ga lattice sites in the LT-GaAs host, Mn_{Ga}, act as acceptors with an impurity binding energy of intermediate strength 0.11 eV [9, 10]. This results in a high hole density, which is assumed to play a crucial role in the hole-mediated ordering of Mn spins [11, 12] On the other hand, Mn atoms occupying interstitial sites of the crystal lattice, Mn_I, act as double donors in GaAs [13] and, together with the native As_{Ga} donors, partially compensate Mn_{Ga} acceptors, thus resulting in effective reduction of the hole concentration in the (Ga, Mn)As films and, in turn, in decreasing their Curie temperature with increasing the Mn content, x, typically both the hole concentration and T_C increase in the as-grown (Ga, Mn)As films up to around $x = 0.06$, beyond which they both start to decrease, primarily due to the formation of Mn interstitials. Post-growth annealing the films at temperatures below the LT-MBE growth temperature, resulting mainly in out-diffusion of the Mn interstitials, allowed for achieving the highest, so far, T_C of 185 K at $x \approx 0.12$[14].

Mn_{Ga} acceptors are more localized than shallower, hydrogenic-like acceptors in GaAs, which results in higher critical carrier density of the metal-insulator transition (MIT) in Mn doped GaAs, of about 1×10^{20} cm^{-3}, as compared to the critical density of two orders of magnitude lower for the shallow acceptors in GaAs [15]. Importantly, a ferromagnetic ordering in (Ga, Mn)As occurs on both the insulating and metallic side of the MIT.

* yastrub@hektor.umcs.lublin.pl

© 2012 Sumy State University

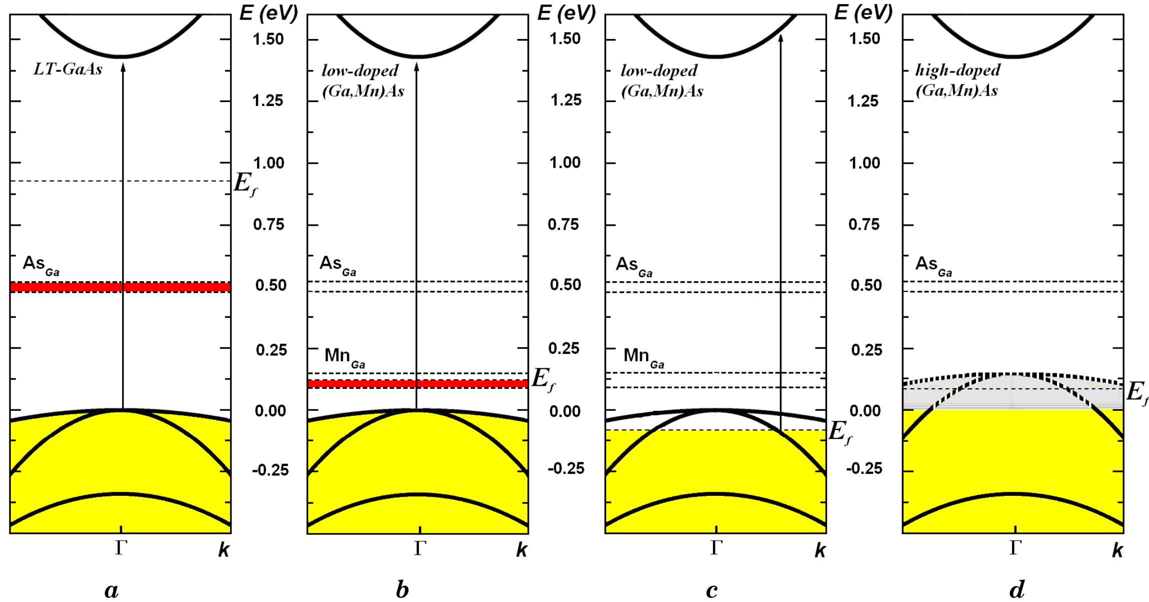

Fig. 1 – Schematic energy band diagram for LT-GaAs (a) and possibilities of its evolution for (Ga,Mn)As with increasing Mn content (b, c, and d). Splitting of the bands in the ferromagnetic state is omitted for simplicity. Arrows indicate electronic transitions from the valence band to the conduction band (E_g). Impurity-band regime for low-Mn-doped (Ga,Mn)As is presented in (b): a narrow impurity band is formed at an energy of the Mn_{Ga} acceptor level, separated from the valence band by an energy gap of the magnitude close to the impurity binding energy, with the Fermi level residing inside this band (assuming some compensation). An alternative scenario is shown (c), where holes are doped into the valence band from Mn_{Ga} acceptor levels and the absorption edge shifts from the center of the Brillouin zone to the Fermi-wave vector. The disordered-valence-band regime for high-Mn-doped (Ga,Mn)As is presented in (d), where the impurity band and the host valence band merge into one inseparable band, whose tail may still contain localized states (shaded grey area) depending on the free carrier concentration and disorder

The nature of conducting carriers mediating the ferromagnetic state in this material has not yet been unambiguously clarified. There are two alternative theories about the electronic structure of metallic (Ga, Mn)As. The first one involves persistence of the Mn_{Ga}-related impurity band on the metallic side of the MIT with the Fermi level residing within the impurity band and mobile holes retaining the impurity band character,[16–18] as shown schematically in Fig. 1b. The second one assumes mobile holes residing in nearly unperturbed valence band of the GaAs host (Fig. 1c), which play a key role in the *p-d* Zener model of ferromagnetism in diluted magnetic semiconductors [11, 12] Elucidation of the above controversy is essential for a better understanding of carrier mediated ferromagnetism phenomenon [19], which is also important in view of potential applications of ferromagnetic semiconductors for spintronic devices. In order to resolve this question, systematic magnetic, optical, and transport experiments have been carried out on (Ga, Mn)As films by many research groups worldwide.

In the present work, fundamental properties of the energy band structure, like intrerband energy transitions and electro-optic energies of LT-GaAs and (Ga,Mn)As films with various Mn contents were determined. The one of modulation spectroscopies – photoreflectance (PR) was applied, as the most precise, nondestructive, and contactless optical characterisation technique. This nonlinear technique allowed to observe clear band-to-band transition, otherwise a strong absorption tail characteristic of low-temperature grown GaAs and (Ga, Mn)As caused by the defect-to-band transitions and masks any Mn-related features near the fundamental band gap observed in linear spectroscopy. Photoreflectance studies were supported by Raman spectroscopy and high resolution X-ray diffractometry (XRD) measurements and magnetic properties of the (Ga, Mn)As films were characterized with a superconducting quantum interference device (SQUID) magnetometer.

2. EXPERIMENTAL

For our investigations two series of the thick 800-700 nm and 300-230 nm ferromagnetic (Ga,Mn)As films with Mn content from 0.001 % and 6 % have been used. The films were grown by means of the LT-MBE method at a temperature of 230 °C on semi-insulating (001)-oriented GaAs substrates. Such heterostructures were chosen because of their different transport and optical properties. While (Ga, Mn)As containing up to 2 % Mn is expected to be close to the MIT, the Mn content higher than 2 % usually transfers (Ga, Mn)As films into metallic state. In addition, as a reference LT-GaAs film, we investigated a 700 nm and 230 nm-thick undoped GaAs film grown on GaAs by LT-MBE under the same conditions as the (Ga, Mn)As films. Both the Mn composition and the film thickness were verified during the growth by the reflection high-energy electron diffraction (RHEED) intensity oscillations, which enabled to determine the composition and film thickness with accuracy of 0.1 % and one monolayer, respectively [20].

The films were subjected to investigations of their properties using several complementary characterization techniques. Magnetic properties and the T_C values for the (Ga,Mn)As films were inspected using both magnetic-field – and temperature-dependent SQUID

magnetometry. Micro-Raman spectroscopy was employed to estimate the hole densities in the thick (Ga, Mn)As films. The micro-Raman measurements were performed using an inVia Reflex Raman microscope (Renishaw) at room temperature with the 514.5-nm argon ion laser line as an excitation source. Structural properties of the thick epitaxial films were investigated by analysis of XRD results obtained at the temperature 27 °C by means of high-resolution X-ray diffractometer equipped with a parabolic X-ray mirror and four-bounce Ge 220 monochromator at the incident beam and a three-bounce Ge analyzer at the diffracted beam. Misfit strain in the epitaxial films was investigated using the reciprocal lattice mapping and the rocking curve techniques for both the symmetric 004 and asymmetric 224 reflections of CuKα_1 radiation.

Room temperature PR measurements were performed using an argon ion laser working at the 488 nm wavelength and a nominal power of 50 mW as a pump-beam source and a 250 W halogen lamp coupled to a monochromator as a probe-beam source. The PR signal was detected by a Si photodiode. The chopping frequency of the pump beam was 70 Hz and the nominal spot size of the pump and probe beams at the sample surface were 2 mm in diameter.

3. RESULTS AND DISCUSSION

Results of SQUID magnetometry applied to the (Ga,Mn)As films showed that they all exhibit an in-plane easy axis of magnetization and well-defined hysteresis loops in their magnetization vs. magnetic field dependence. The films of 230 nm thickness displayed T_C values of 40 K and 60 K for a Mn content of 1% and 6 %, respectively. The (Ga, Mn)As films of 300 nm thickness with a Mn content of 2% and 4% displayed T_C values of 50 K and 60 K, respectively. This range of Curie temperature is typical for unannealed, relatively thick (Ga,Mn)As films [4].

SQUID magnetometry have revealed the non-ferromagnetic character of the ultra low (0.001 % and 0.005%) doped (Ga, Mn)As 700-800 nm epitaxial layers. Due to the small amount of Mn atoms we have assumed that free holes concentration is too weak or lacking at all to induce the ferromagnetic effect. This suggestion was supported by the thermoelectric power measurements, which revealed that (Ga, Mn)As epitaxial layers with ultra low Mn concentration exhibit *n*-type conductivity.

The micro-Raman spectra obtained for the LT-GaAs and (Ga, Mn)As films of 230 nm and 800-700 nm thicknesses are presented in Fig. 2. Quantitative analysis of Raman spectra can provide important information about the free-carrier density. Seong et al. [21] proposed a powerful procedure, which enables for accurate determining the carrier density without necessity of applying large magnetic fields, as is required in the Hall-effect measurements for ferromagnetic materials.

In (Ga, Mn)As films, characterized by a high density of free holes of about 10^{20} cm^{-3}, the interaction between the hole plasmon and the LO phonon leads to the formation of coupled plasmon-LO phonon (CPLP) mode [22]. In addition, it results in a broadening and a shift of the Raman line from the LO-phonon position to the TO-

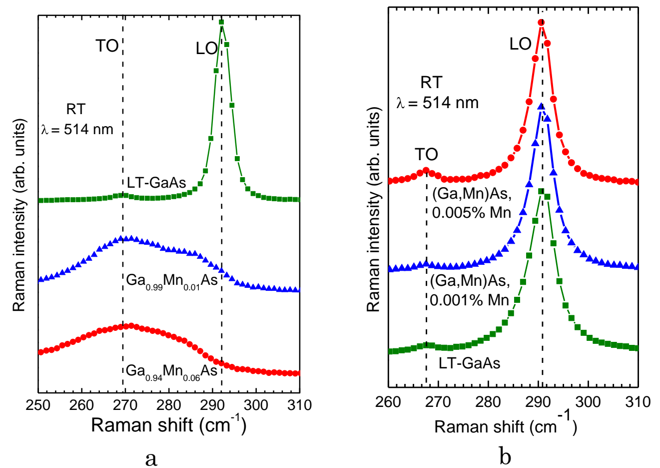

Fig. 2 – Raman spectra recorded at room temperature in backscattering configuration from the (001) surfaces of the 230-nm LT-GaAs reference and two (Ga,Mn)As films with Mn content 1% and 6% (***a***) and 800-700nm LT-GaAs reference and two (Ga,Mn)As films with Mn content 0.001 % and 0.005 % (b). The spectra have been vertically offset for clarity. The dashed lines indicate the positions of the Raman LO- and TO-phonon lines for the LT-GaAs reference films

phonon position depending on the hole density [23] From micro-Raman spectra we have estimated the hole concentrations of 0.9×10^{20} cm^{-3} and 1.4×10^{20} cm^{-3} in the films with the Mn content of 1 % and 6%, respectively (Fig. 2a). The obtained results suggest that the first (Ga, Mn)As film demonstrates properties of insulator-like material and the second one does those of metallic-like material.

Contrary to this the micro-Raman spectra measured for 800-700 nm (Ga, Mn)As epitaxial films with ultra low Mn content (Fig. 2b) did not indicate any changes in LO and TO phonon position with respect to the reference LT-GaAs epitaxial layer. The CPLP phonon mode was not observed as well. It suggests that the structural and electronic properties of LT-GaAs and (Ga,Mn)As epitaxial films with ultra low Mn content are very similar.

Our results of high-resolution XRD measurements revealed that both the LT-GaAs and (Ga,Mn)As films, grown on GaAs substrate under compressive misfit stress, were fully strained to the (001) GaAs substrate. The film thicknesses calculated from the angular spacing of the fringes correspond very well to their thicknesses determined from the growth parameters. The lattice unit of the films changes with increasing lattice mismatch from the zinc-blende cubic structure to the tetragonal structure with the perpendicular lattice parameter larger than the lateral one, equal to the GaAs lattice parameter.

Photoreflectance study presented in this paper is probably the first experimental observation of the fundamental energy gap in (Ga, Mn)As films with very bright range from 0.001 % to 6 % of Mn content. Owing to derivative nature of PR spectroscopy it allows for accurate determination of the band-gap energies even at room temperature. As the PR signal is associated with the electric field caused by the separation of photogenerated charge carriers, its intensity significantly decreases in highly doped semiconductors because of

efficient screening of the electric field by free carriers. Accordingly, the intensity of the measured PR signal strongly decreased with increasing Mn content in the investigated films. This intensity for the $Ga_{94}Mn_{06}As$ sample was smaller by about one order of magnitude than that for the LT-GaAs sample. That is why the spectra presented in Fig. 3 have been normalized to the same intensity.

The PR spectra measured in the photon-energy range from 1.30 to 1.70 eV for both the LT-GaAs and (Ga,Mn)As epitaxial films reveal a rich, modulated structure containing two main features: electric-field-induced Franz-Keldysh oscillations (FKO) at energies above the fundamental absorption edge and a peak at around the GaAs energy gap. Some of the spectra reveal a below-band-gap feature. Despite the thicknesses of our epitaxial films (from 800 to 230 nm) are larger than the penetration depth of 488-nm argon-ion-laser line in crystalline GaAs, estimated to about 100 nm [24], we were able to detect a PR-signal contribution coming from the film-substrate interface regions for 300-230 nm layers (Fig. 3a,b). This contribution results from a transport of laser-injected carriers to the interface and formation of space-charge volume, which extends in GaAs to 1 μm in depth. Sydor et al. [24] associated the below-band-gap feature in their PR signal from MBE-grown GaAs thin films on GaAs substrate with impurity effects at the GaAs/GaAs interface. According to their interpretation, the modulation mechanism of this feature results from the thermal excitation of impurities or traps at the interface and their momentary refilling by the laser-injected carriers. In line with this interpretation, amplitudes of the below-band-gap feature in our PR results decrease with the increasing of the thicknesses of the films (Fig. 3a,b) and disappear at all for very thick (800-700 nm) layers (Fig. 3c).

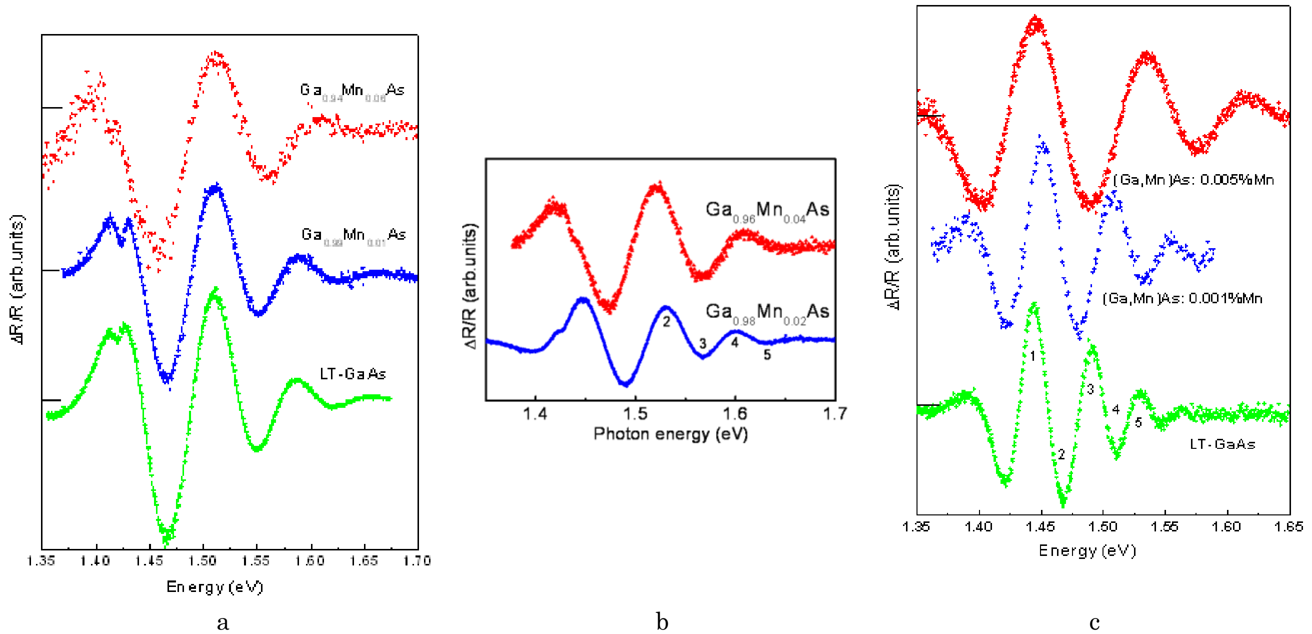

Fig. 3 – Sequence of the photoreflectance spectra for the LT-GaAs, (Ga,Mn)As films epitaxially grown on GaAs substrate: ***(a)*** 230 nm LT-GaAs, $Ga_{0.99}Mn_{0.01}As$, and $Ga_{0.94}Mn_{0.06}As$; (b) 300 nm $Ga_{0.98}Mn_{0.02}As$ and $Ga_{0.96}Mn_{0.04}As$; (c) 800-700 nm LT-GaAs, (Ga, Mn)As: 0.001% Mn, and (Ga, Mn)As: 0.005% Mn. The curves have been vertically offset for clarity

From analysis of the FKO periods we obtained the interband transition energies E_g in (Ga, Mn)As layers with various Mn contents (Fig. 4). This approach neglects the light-hole contribution to PR spectra and takes the asymptotic expression of the Airy function [25]. Using this simplified analysis the value of E_g connected with the nominal band-gap energy is obtained from the intersection with ordinate of the linear dependence of the energies of FKO extrema E_m vs. their "effective index" defined as $F_m = [3\pi(m - 1/2)/4]^{2/3}$:

$$E_m = E_g + \hbar\theta F_m,$$

where m is the extremum number and the electro-optic energy $\hbar\theta$ is defined as $\hbar\theta = (e^2\hbar^2F^2/2\mu)^{1/3}$, where F is the electric field and μ is the interband reduced effective mass [24].

The results of this analysis, neglecting the FKO extremum for $m = 1$, which is affected by the multiple lower-energy features in the PR spectra for the 230 and 300nm-thick films are presented in Fig. 4a,b. The same simplified analysis of the PR spectra with the taking into consideration all the FKO extrema for thick 800-700 nm films is shown in Fig. 4c.

Owing to excitonic nature of the room-temperature PR signal the measured energies of interband transitions are smaller than the nominal band-gap energies by approximately the excitonic binding energy. Thus, the energies obtained from FKO analysis are called critical-point energies rather than the band-gap energies. Thorough analysis of the obtained results shows a blue shift, up to 20 meV, of the E_g transition in $Ga_{0.98}Mn_{0.02}As$ films with respect to the reference LT-GaAs film. In contrast, a substantial red shift, of 40 meV, of the E_g energy, equal to 1.386 eV, was revealed for the $Ga_{0.94}Mn_{0.06}As$ film. Such an effective reduction of the energy gap in highly Mn-doped

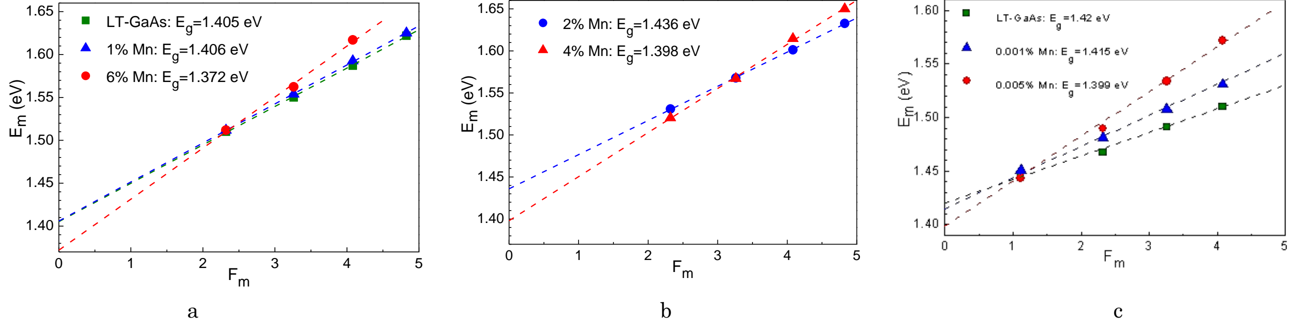

Fig. 4 – Analysis of the period of Franz-Keldysh oscillations for (a) 230 nm LT-GaAs, $Ga_{0.99}Mn_{0.01}As$, and $Ga_{0.94}Mn_{0.06}As$ films; (b) 300 nm $Ga_{0.98}Mn_{0.02}As$, and $Ga_{0.96}Mn_{0.04}As$ films and (c) 700-800 nm LT-GaAs, (Ga, Mn)As: 0.001% Mn, (Ga,Mn)As: 0.005% Mn. The values of E_g obtained from the analysis are listed in the figures. The numbers of the FKO extrema used for the analysis are marked on Fig. 3

(Ga, Mn)As film is in qualitative agreement with the results of STS [26, 27], which suggested even smaller band gap of 1.23 eV in (Ga, Mn)As film with 3.2 % Mn content, as estimated from conductance spectra measured in the scanning tunneling microscope [26]. Large difference between that result and our experimental value of the E_g energy may result from different measurement techniques used and a limited energy resolution of the STS technique.

Our PR results evidence a tangible difference in the electronic band structures of (Ga, Mn)As with low and high Mn contents. The blue shift of E_g transition in the $Ga_{0.99}Mn_{0.01}As$ and $Ga_{0.98}Mn_{0.02}As$ film indicates the Fermi level position below the top of GaAs valence band, which is consistent with the situation presented in Fig. 1c, where the E_g transition occurs from the Fermi level to the conduction band. Then, the small increase of the E_g energy may result from the Moss-Burstein shift of the absorption edge [28].

On the other hand, significant red shift of the E_g transition in the (Ga, Mn)As films with high 4 % and 6% Mn contents is consistent with the band structure presented in Fig. 1d, where the Mn-related impurity band is merged with the GaAs valence band, forming a disordered valence band extended within the band gap [15]. In this case the E_g transition occurs from the Fermi level in the disordered valence band to the conduction band. The red-shift magnitude of the E_g transition results from interplay between the band-gap narrowing and the Moss-Burstein shift in highly Mn-doped (Ga, Mn)As. Moreover, a lack of splitting of the PR spectra into light- and heavy-hole features in the spectral area near the E_g transition, even in the $Ga_{0.94}Mn_{0.06}As$ film with a vertical strain as high as 4.2×10^{-3} (from XRD results), may be explained by the disordered character of valence band in this case [29].

The slight red shift of the E_g transition in (Ga, Mn)As epitaxial layers with ultra low Mn concentration with respect to the reference LT-GaAs film could not be explained by the structural changes of Mn-doped layers, because Mn concentrations are to small to have the significant impact on the structural properties of the epitaxial layers. That was confirmed by the micro-Raman and HR XRD measurements [30].

This red shift of the E_g transition could be caused by the compensation character of the conductivity in ultra low doped (Ga, Mn)As films. Probably the Moss-Burstein effect impacts partially on the electronic properties of the undoped LT-GaAs films at the room temperature as well, because of a large number of defects arising during the LT MBE growth. These defects, mainly As_{Ga} with a typical concentration of 1×10^{20} cm^{-3}, determine the electronic structure of LT-GaAs.

In the (Ga, Mn)As epitaxial layers Mn atoms substitute the Ga lattice sites in the LT-GaAs host, Mn_{Ga}, and act as acceptors with an impurity binding energy of intermediate strength 0.11eV, what results in a high hole density, which is assumed to play a crucial role in the holemediated ordering of Mn spins. When the Mn concentration is extremely low, we probably observe only the decreasing of number of the unoccupied states near the conduction band. In this case (Ga, Mn)As are n-type and does not show any ferromagnetic behaviour. That is why the transition critical point energy in (Ga, Mn)As n-type epitaxial layers with ultra low Mn contents lightly decrease as long as this material do not transfer with the increasing of Mn concentration into the p-type. In this case the Fermi level in (Ga, Mn)As shifts from the band-gap into the valence band (see Fig. 1c), and when Mn concentration exceeds 1 %, (Ga, Mn)As epitaxial layers become ferromagnetic.

4. CONCLUSIONS

In this work we have employed complementary characterization techniques, such as photoreflectance spectroscopy, Raman spectroscopy, high resolution X-ray diffractometry, and SQUID magnetometry, for revealing the fundamental properties of (Ga,Mn)As epitaxial films with different Mn content. Our PR spectroscopy measurements enabled determination of the E_g electronic transition in (Ga,Mn)As and its dependence on the Mn content.

In (Ga, Mn)As with ultra low (0.001-0.005 %) Mn concentration the transition energy is slightly red shifted with respect to that in reference LT-GaAs, which was interpreted as a result of the compensation character of the conductivity in these *n*-type, non ferromagnetic epitaxial layers. The Fermi level in such (Ga, Mn)As is located in the band gap.

In *p*-type (Ga,Mn)As with a low (1-2 %) Mn content and hole density close to that of the MIT, the interband transition energy was blue shifted with respect to that in reference LT-GaAs, which was interpreted as a re-

sult of the Moss-Burstein shift of the absorption edge due to the Fermi level location below the top of GaAs valence band. On the other hand, a substantial red shift, of 40 meV, of the E_g energy was revealed in (Ga, Mn)As with the highest (6%) Mn content and a hole density corresponding to metallic side of the MIT. This result, together with the determined other parameters of the intrerband electro-optic transitions near the center of the Brillouin zone, which were significantly different from those in reference LT-GaAs, was interpreted in terms of a disordered valence band, extended within the band-gap, formed in highly Mn-doped (Ga, Mn)As as a result of merging the Mn-related impurity band with the host GaAs valence band.

ACKNOWLEDGEMENTS

O. Y. acknowledges financial support from the Foundation for Polish Science under Grant POMOST/2010-2/12 sponsored by the European Regional Development Fund, National Cohesion Strategy: Innovative Economy. Author thanks Dr. hab. J. Sadowski for samples sharing, Dr. J.Z. Domagala for HR XRD measurements, and Prof. Wosinski and Prof. Zuk for productive discussions.

REFERENCES

1. S. Mack, R.C. Myers, J.T. Heron, A.C. Gossard, D.D. Awschalom, *Appl. Phys. Lett.* **92**, 192502 (2008).
2. M. Kaminska, Z. Liliental-Weber, E.R. Weber, T. George, J.B. Kortright, F.W. Smith, B.-Y. Tsaur, A.R. Calawa, *Appl. Phys. Lett.* **54**, 1881 (1989).
3. D.C. Look, D.C. Walters, M.O. Manasreh, J.R. Sizelove, C.E. Stutz, K.R. Evans, *Phys. Rev. B* **42**, 3578 (1990).
4. E.R. Weber, H. Ennen, U. Kaufmann, J. Windschief, J. Schneider, T. Wosinski, *J. Appl. Phys.* **53**, 6140 (1982).
5. H. Shen, F.C. Rong, R. Lux, J. Pamulapati, M. Taysing-Lara, M. Dutta, E.H. Poindexter, L. Calderon, Y. Lu, *Appl. Phys. Lett.* **61**, 1585 (1992).
6. S. Lodha, D.B. Janes, N.-P. Chen, *J. Appl. Phys.* **93**, 2772 (2003).
7. R.M. Feenstra, J.M. Woodall, G.D. Pettit, *Phys. Rev. Lett.* **71**, 1176 (1993).
8. E.J. Singley, K.S. Burch, R. Kawakami, J. Stephens, D.D. Awschalom, D.N. Basov, *Phys. Rev. B* **68**, 165204 (2003).
9. R.A. Chapman, W.G. Hutchinson, *Phys. Rev. Lett.* **18**, 443 (1967).
10. A.M. Yakunin, A.Yu. Silov, P.M. Koenraad, J.H. Wolter, W. Van Roy, J. De Boeck, J.-M. Tang, M.E. Flatté, *Phys. Rev. Lett.* **92**, 216806 (2004).
11. T. Dietl, H. Ohno, F. Matsukura, *Phys. Rev. B* **63**, 195205 (2001).
12. T. Jungwirth, J. Sinova, J. Mašek J. Kučera, A.H. Mac Donald, *Rev. Mod. Phys.* **78**, 809 (2006).
13. K.M. Yu, W. Walukiewicz, T. Wojtowicz, I. Kuryliszyn, X. Liu, Y. Sasaki, J.K. Furdyna, *Phys. Rev. B* **65**, 201303(R) (2002).
14. M. Wang, R.P. Campion, A.W. Rushforth, K.W. Edmonds, C.T. Foxon, B.L. Gallagher, *Appl. Phys. Lett.* **93**, 132103 (2008).
15. T. Jungwirth, J. Sinova, A.H. Mac Donald, B.L. Gallagher, V. Novák, K.W. Edmonds, A.W. Rushforth, R.P. Campion, C.T. Foxon, L. Eaves, E. Olejník, J. Mašek, S.-R. Eric Yang, J. Wunderlich, C. Gould, L.W. Molenkamp, T. Dietl, H. Ohno, *Phys. Rev. B* **76**, 125206 (2007).
16. M. Berciu, R.N. Bhatt, *Phys. Rev. B* **69**, 045202 (2004).
17. K.S. Burch, D.B. Shrekenhamer, E.J. Singley, J. Stephens, B.L. Sheu, R.K. Kawakami, P. Schiffer, N.Samarth, D.D. Awschalom, D.N. Basov, *Phys. Rev. Lett.* **97**, 087208 (2006).
18. B.L. Sheu, R.C. Myers, J.-M. Tang, N. Samarth, D.D. Awschalom, P. Schiffer, M.E. Flatté, *Phys. Rev. Lett.* **99**, 227205 (2007).
19. A. Richardella, P. Roushan, S. Mack, B. Zhou, D.A. Huse, D.D. Awschalom, A. Yazdani, *Science* **327**, 665 (2010).
20. J. Sadowski J.Z. Domagała, J. Bąk-Misiuk, S. Koleśnik, M. Sawicki, K. Świątek, J. Kanski, L. Ilver, and V. Ström, *J. Vac. Sci. Technol. B* **18**, 1697 (2000).
21. M.J. Seong, S.H. Chun, H.M. Cheong, N. Samarth, A. Mascarenhas, *Phys. Rev. B* **66**, 033202 (2002).
22. G. Irmer, M. Wenzel, J. Monecke, *Phys. Rev. B* **56**, 9524 (1997).
23. W. Limmer, M. Glunk, W. Schoch, A. Köder, R. Kling, R. Sauer, A. Waag, *Physica E* **13**, 589 (2002).
24. M. Sydor, J. Angelo, J.J. Wilson, W.C. Mitchel, M.Y. Yen, *Phys. Rev. B* **40**, 8473 (1989).
25. D.E. Aspnes, A.A. Studna, *Phys. Rev. B* **7**, 4605 (1973).
26. T. Tsuruoka, N. Tachikawa, S. Ushioda, F. Matsukura, K. Takamura, H. Ohno, *Appl. Phys. Lett.* **81**, 2800 (2002).
27. G. Mahieu, P. Condette, B. Grandidier, J.P. Nys, G. Allan, D. Stiévenard, Ph. Ebert, H. Shimizu, M. Tanaka, *Appl. Phys. Lett.* **82**, 712 (2003).
28. K.M. Yu, W. Walukiewicz, T. Wojtowicz, W.L. Lim, X. Liu, U. Bindley, M. Dobrowolska, J.K. Furdyna, *Phys. Rev. B* **68**, 041308(R) (2003).
29. O. Yastrubchak J. Żuk, H. Krzyżanowska, J. Z. Domagala, T. Andrearczyk, J. Sadowski, and T. Wosiński, *Phys. Rev. B* 83, 245201 (2011).
30. O. Yastrubchak J. Żuk, J.Z. Domagala, L. Gluba, J. Sadowski, T. Wosiński, *1-st NAP (Nanomaterials: Applications & Properties) Proceedings* **1** Part II, 328 (2011).